Topics in Catalysis manuscript No.
(will be inserted by the editor)

Adsorption and catalytic activation of the molecular oxygen on the metal supported h-BN

Andrey Lyalin · Akira Nakayama · Kohei Uosaki · Tetsuya Taketsugu

Received: date / Accepted: date

Abstract Adsorption and catalytic activation of the molecular oxygen on the hexagonal boron nitride (h-BN) monolayer supported on Ni(111) and Cu(111) surfaces have been studied theoretically using density functional theory. It is demonstrated that an inert h-BN monolayer can be functionalized and become catalytically active on the transition metal support as a result of mixing of the metal d and h-BN π bands.

Keywords oxidation reactions · oxygen activation · oxygen adsorption · hexagonal boron nitride · nickel · copper

This work was supported by Elements Science and Technology Project of Ministry of Education, Culture, Sports, Science and Technology, Japan (MEXT) on "Nano-hybridized Precious-metal-free Catalysts for Chemical Energy Conversion". A part of this work was performed under a management of "Elements Strategy Initiative for Catalysts & Batteries (ESICB) " supported by MEXT program "Elements Strategy Initiative to Form Core Research Center" (since 2012). The computations were partly performed using the computer facilities of ESCIB, Kyoto and the Research Center for Computational Science, Okazaki, Japan.

A. Lyalin
Elements Strategy Initiative for Catalysts and Batteries (ESICB), Kyoto University, Kyoto 615-8245, Japan
E-mail: lyalin@esicb.kyoto-u.ac.jp
On leave from: V. A. Fock Institute of Physics, St Petersburg State University, 198504 St Petersburg, Petrodvorez, Russia

A. Nakayama
Catalysis Research Center, Hokkaido University, Sapporo 001-0021, Japan

K. Uosaki
International Center for Materials Nanoarchitechtonics (WPI-MANA), National Institute for Materials Science (NIMS), Tsukuba 305-0044, Japan

T. Taketsugu
Department of Chemistry, Faculty of Science, Hokkaido University, Sapporo 060-0810, Japan
Elements Strategy Initiative for Catalysts and Batteries (ESICB), Kyoto University, Kyoto 615-8245, Japan
E-mail: take@sci.hokudai.ac.jp

1 Introduction

The reactions of selective oxidation are among the most important processes in many chemical and industrial applications. Often such reactions involve several stages with the use of chlorine or organic peroxides resulting in a production of toxic by-products and waste [1]. Therefore, many efforts are underway to develop efficient green alternatives to traditional, toxic chemical oxidants [2]. One of the promising approach in this direction is nanocatalysis, which considers selective oxidation by the molecular oxygen on supported metal nanoparticles [3]. Using molecular oxygen as an oxidizing agent can make oxidation process an ideal and waste free reaction [1]. For example, it has been demonstrated that nanoparticles of gold have exceptional catalytic properties in oxidation reactions, including the oxidation of carbon monoxide at mild temperatures, alcohol oxidation, the direct synthesis of hydrogen peroxide and alkene epoxidation [4–10]. These unique properties of gold emerge when the size of catalytic particles decreases down to 1-5 nm; while larger sized particles and the bulk form of gold are catalytically inactive [4–6, 8]. Thus, an inert gold becomes catalytically active at nanoscale.

There are two possible routes for catalytic oxidation on the surface of metal nanoparticles. The first route consists in a preliminary dissociation of the adsorbed molecular O_2 followed by consequential oxidation of a reactant molecule by atomic oxygen. The second route is a direct oxidation reaction between an activated O_2 and a reactant molecule [11, 12]. The process of direct oxidation by the activated molecular oxygen seems to be preferable, because it is difficult to control the reactivity of the dissociated oxygen species on metal nanoparticles [1].

Although catalysis by gold nanoparticles is a very promising approach, gold and other transition metals (Pt, Pd, Ru, etc.) widely used in nanocatalysis are expensive for industrial applications. Therefore development of effective and environment friendly catalysts based on the non-precious abundant elements is emerging task.

In this work we present theoretical investigation on very unusual catalytic properties of the material that traditionally was believed to be inert. We demonstrate that chemically inert hexagonal boron nitride (h-BN) monolayer can be functionalized and become catalytically active for oxygen activation.

Until recently, the hexagonal BN has never been considered as a possible catalyst, due to its wide band gap of 5-6 eV and high thermal and chemical stability [13]. However, electronic properties of the low-dimensional h-BN systems differ considerably from those known for the h-BN bulk. The band gap in a h-BN monolayer can be considerably reduced by vacancy and impurity defects due to appearance of the defect states in the forbidden zone of h-BN [14–17]. The point defects can also induce the spin polarization and spontaneous magnetization of the h-BN lattice [15, 16]. Such modifications of the h-BN electronic structure can result in the promotion of interaction between molecules or clusters with the defected h-BN surface.

Recently, we have demonstrated that small gold particles can be trapped effectively by N or B vacancy or impurity point defects in h-BN. Strong adsorption on the surface defects is accompanied by the charge transfer to/from the adsorbate which can affect the catalytic activity of gold [18]. It has been shown that interaction of Au with the h-BN surface can affect considerably the pathways and barriers of CO oxidation reaction by molecular oxygen [19]. Moreover, adsorption,

activation and dissociation of O_2 on h-BN supported gold atoms and dimers can be affected even by the interaction with the defect-free inert h-BN support via the electron pushing mechanism [16–18]. Although the defect-free h-BN surface does not act as a good electron donor for the supported O_2-Au, it promotes an electron transfer from the Au to O_2, pushing electrons from the gold to the adsorbed oxygen. This effect occurs due to the mixing of the 5d orbitals of the supported gold with the N-p_z orbitals [16–18]. It has been shown, that O_2 chemisorbs on the nitrogen impurity, N_B, boron impurity, B_N, nitrogen vacancy, V_N, and boron vacancy, V_B, point defects with the binding energy of 0.24 eV, 1.62 eV, 3.10 eV, and 1.96 eV, respectively [13]. Interaction of O_2 with the point defects in h-BN monolayer results in activation of the adsorbed O_2 and weakening of the O−O bond. The O−O bond length in O_2 adsorbed on N_B, B_N, and V_N defects in h-BN is enlarged similar to the superoxide state of oxygen (the O−O bond distances in O_2^- is 1.33 Å[20]). In the case of O_2 adsorption on the V_B defect in h-BN monolayer oxygen molecule is partially dissociated with the distance between O atoms of 1.79 Å. Activation of the adsorbed O_2 is accompanied by the charge transfer from the defected surface to the oxygen. Such mechanism of the charge-transfer-mediated activation of O_2 has been intensively studied for O_2 adsorbed on metal clusters; see, *e.g.*, [11, 18, 21–27] and references therein. As it was discussed in [13] the h-BN monolayer with B_N, V_N, and V_B defects can not be a good catalyst due to the strong bonding of O_2 to the surface. However, N-doped h-BN monolayer demonstrates catalytic activity for the oxygen reduction reaction [13].

Support effects can significantly modulate the band gap in two-dimensional (2D) nanostructures. Much attention has been paid to h-BN monolayer adsorbed on transition metal surfaces because of possible applications in nano-electronics and chemistry, see, e.g., [28–30] and references therein. Results of experimental and theoretical studies on the electronic properties of h-BN monolayer adsorbed on transition metal surfaces are still very controversial. In earlier experiments by angle resolved ultraviolet photoelectron spectroscopy and angle resolved secondary-electron spectroscopy, it was found that h-BN monolayer is weakly bound to the metal surfaces and remains insulator [31]. However, in later experiments performed by the same group using the high resolution electron loss spectroscopy some mixing of the π h-BN and d metal bands has been reported [32]. On the other hand near-edge x-ray adsorption fine structure, photoemission and Auger spectroscopy demonstrate strong orbital hybridization between Ni 3d and h-BN π states, which indicates strong interaction between h-BN and Ni(111) substrate [33–35]. The analysis of the electronic structure of the bulk h-BN and the h-BN/Ni(111) interface demonstrates that the gap between bonding and antibonding states of h-BN monolayer on Ni(111) surface becomes filled mostly by the N-p_z and B-p_z states due to a strong interaction with the metal d-band [36, 37]. Theoretical calculations show that the electronic and magnetic properties of a h-BN monolayer supported on 3d, 4d and 5d transition metal surfaces can be modified as a result of mixing of the d_{z^2} metal orbitals with N-p_z and B-p_z orbitals of the h-BN monolayer [28, 37–42].

It is known that adsorption and activation of O_2 on the catalytic surface can be strongly affected by the density of electronic states (DOS) near the Fermi level of the catalyst. Therefore, the metal substrate can influence on the molecular adsorption and chemical reactions on the supported h-BN surface due to the mixing between metal d and h-BN π bands. Such an effect can open a new way to tune

adsorption characteristics of O_2 and reactant molecules on h-BN by the selection of metal substrate.

In the present work we present results of a theoretical investigation of the binding preference and catalytic activation of O_2 adsorbed on the h-BN monolayer supported on the Ni(111) and Cu(111) surfaces. We show that h-BN/metal systems can possess very interesting catalytic activity for oxygen activation as a result of mixing of the metal d and h-BN π bands.

2 Methods

The calculations are carried out using density-functional theory (DFT) with the gradient-corrected exchange-correlation functional of Wu and Cohen (WC) [43]. The choice of DFT method is stipulated by the fact that the WC functional provides a good description of the lattice constants, crystal structures and surface energies of solids with layered structures like graphite or h-BN, whose distances between the layers are determined by rather weak interactions [44]. Moreover, the WC functional gives a realistic description of the binding energies and geometries of h-BN layer on top of 3d, 4d and 5d transition metal surfaces, correctly describing the interaction of transition metals with h-BN [37, 44, 45]. The WC functional was successfully used in our previous works to describe ORR on N-doped h-BN monolayer [13], and catalytic activity of small gold particles on the pristine and defected h-BN surfaces [16, 17, 19].

Double-ζ plus polarization function (DZP) basis sets are used to treat the $2s^2 2p^1$, $2s^2 2p^3$, $2s^2 2p^4$, $3d^8 4s^2$ and $3d^{10} 4s^1$ valence electrons of B, N, O, Ni and Cu atoms, respectively [46, 47]. The core electrons are represented by the Troullier-Martins norm-conserving pseudopotentials [48] in the Kleinman-Bylander factorized form [49]. All calculations have been carried out with the use of the SIESTA package [50–52]. Periodic boundary conditions are used for all systems, including free molecules. In the latter case the size of a supercell was chosen to be large enough to make intermolecular interactions negligible. The h-BN and metal (Ni, Cu) lattices have been optimized using the Monkhorst-Pack [53] 10×10×4 and 10×10×10 k-point mesh for Brillouin zone sampling, respectively. The calculated h-BN lattice parameters a = b = 2.504 Å and c = 6.656 Å are in a good agreement with the experimental values of a = b = 2.524 ± 0.020 Å and c = 6.684 ± 0.020 Å, reported in [54]. The calculated lattice parameters of Ni and Cu face-centered cubic (fcc) bulk structures are a = 3.524 and 3.626 Å, respectively. The obtained lattice parameters of Ni and Cu are in the excellent agreement with the experimental data of 3.5238 [55] and 3.6149 Å [56], respectively.

The optimized lattices of the bulk Ni and Cu were used to construct slabs for h-BN/Ni(111) and h-BN/Cu(111) surfaces, respectively. The four-layer slabs containing 6×6 unit cells (144 atoms per slab) represent the Ni(111) and Cu(111) surfaces. The calculated lattice parameter of h-BN monolayer 2.504 Å has a close value with the surface lattice constants of Ni(111), 2.492 Å and Cu(111), 2.564 Å, resulting in a good match of the h-BN, Ni(111) and Cu(111) lattices. The periodically replicated slabs are separated by the vacuum region of 20 Å. In calculations the bottom three layers in the slabs are fixed, and all other atoms are fully relaxed. Only the Γ point is used for the Brillouin zone sampling due to the large size of the supercell. The energy cutoff of 200 Ry is chosen to guarantee convergence of

the total energies and forces. A common energy shift of 10 meV is applied. The self-consistency of the density matrix is achieved with a tolerance of 10^{-4}. For geometry optimization the conjugate-gradient approach was used with a threshold of 0.02 eV $Å^{-1}$. The atoms in molecules method of Bader (AIM) has been used for charge analysis [57, 58]. In order to obtain the most stable configuration of the adsorbed O_2 we have generated a large number of starting geometries. The starting structures have been optimized without any geometry constraints. The similar approach has been successfully used in our previous works for oxygen reduction reaction on the N-doped h-BN monolayer [13], on adsorption of O_2, H_2, and C_2H_4 molecules on the free and supported gold clusters [11, 12, 16, 17, 19, 59, 60] as well as on molecular and cluster structure optimization [61–65].

3 Results and discussion

3.1 Geometry and electronic structure of a pristine h-BN monolayer, and h-BN monolayer deposited on Ni(111) and Cu(111) metal surfaces.

Adsorption and activation of O_2 on the catalytic material is one of the most important steps for oxidation reactions by molecular oxygen. In the present work we study several possible sites for O_2 adsorption on h-BN monolayer deposited on the Ni(111) and Cu(111) surfaces. The considered surface models are schematically shown in Figure 1.

Structure and stability of h-BN on transition metal surfaces have been a subject of many theoretical [28, 37–39, 66] and experimental [31, 33–35, 41, 67, 68] studies. Our calculations demonstrate that the most stable configuration of h-BN on Ni(111) is that with N atoms on top of the Ni atoms in the first metal layer with the N-Ni distance of 2.11 Å, while B atoms are located on top of the fcc hollow sites on the surface in accord with the previous theoretical studies [37, 38]. The calculated binding energy of h-BN monolayer to Ni(111) surface is 0.36 eV per BN pair, which is in a reasonable agreement with the theoretical data of 0.19 eV [37] and 0.39 eV [28] obtained with the use of WC [43] and revPBE+D3 [69, 70] DFT functionals, respectively. Another possible configuration, where N atoms are located on top of Ni atoms and B atoms occupy the hcp hollow sites instead of fcc sites is less favorable energetically by 13 meV per BN pair. The optimized geometry structure of the h-BN monolayer on the Cu(111) surface is similar to that obtained for the h-BN/Ni(111) system – the N atoms are located on top of the metal atoms in the first surface layer with the N-Cu distance of 2.65 Å, while B atoms are located on top of the fcc hollow sites. The interaction of h-BN monolayer with the Cu(111) surface is much weaker than with the Ni(111) support – the calculated binding energy of h-BN to the Cu(111) surface is only 0.07 eV per BN pair. Therefore the N-Cu interatomic distances are considerably larger than N-Ni ones. Since the lattice constant of h-BN matches almost perfectly with the lattice constants of Ni(111) and Cu(111) surfaces there is no large geometric corrugation of the h-BN monolayer upon its adsorption on Ni(111) and Cu(111). However, h-BN monolayer on Ni(111) is buckled by 0.12 Å, with B atoms closer to the metal surface than N atoms. In the case of Cu(111) support the buckling of the adsorbed h-BN monolayer is only 0.03 Å. One should note that although h-BN monolayer on the Cu(111) surface is not corrugated geometrically, the corrugation of the h-BN

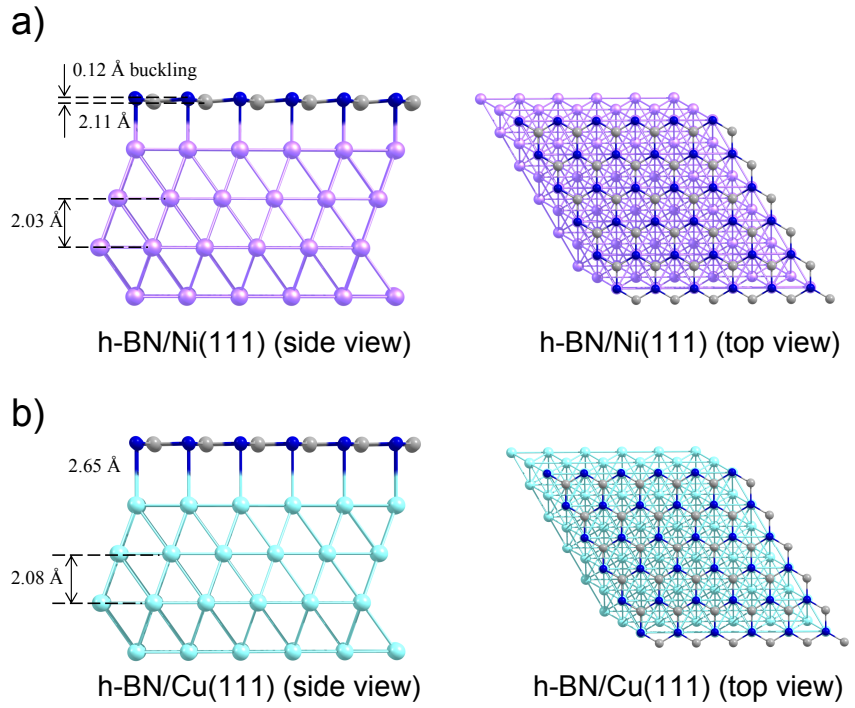

Fig. 1 Surface models: side (left) and top (right) views of the optimized h-BN/Ni(111) (a) and h-BN/Cu(111) (b) structures. All distances are given in Angstroms.

electronic structure and formation of the electronic Moire-like superstructure in h-BN/Cu(111) system has been reported in [71]. Overall, the optimized structures of h-BN/Ni(111) and h-BN/Cu(111) are in a good agreement with the available experimental data [72, 73] and results of previous theoretical calculations [37, 38].

To gain more insight into the electronic structure of the considered h-BN based systems we have calculated the spin polarized DOS which are presented in Figure 2. Our calculations demonstrate that the defect-free h-BN monolayer has a wide band gap of 4.6 eV. Experimental values of the band gap energy for solid h-BN are widely dispersed in the range between 3.6 and 7.1 eV depending on the experimental method [74]. Recent results obtained from the analysis of laser-induced high-resolution fluorescence excitation spectrum of h-BN powder have determined the band gap energy of the solid h-BN: $E_g = 4.02 \pm 0.01$ eV [74].

Figure 2 shows that the PDOS of h-BN monolayer adsorbed on Ni(111) is strongly modified due to interaction with the metal, demonstrating the appearance of the significant density of both occupied and unoccupied gap states with the N-p_z and B-p_z characters. Such an effect occurs due to mixing of the Ni-d_{z^2} orbitals with N-p_z and B-p_z orbitals of the h-BN monolayer in a full agreement with the results of previous theoretical calculations [36, 37]. One can also notice a spin polarization effect, which shifts the down-spin PDOS to the slightly higher energies and resulting in some differences in the up-spin and down-spin gap states. Similar effect has been discussed in [28] and references therein. The existence

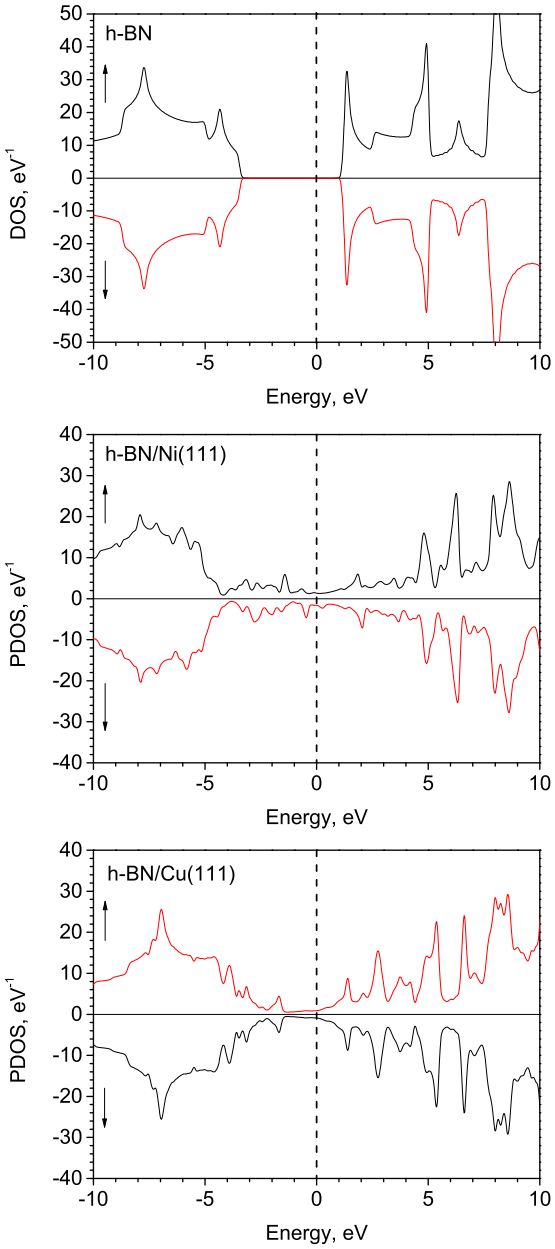

Fig. 2 Spin polarized density of electronic states (DOS) calculated for the defect free h-BN monolayer as well as partial DOS (PDOS) projected on B and N atoms for h-BN/Ni(111) and h-BN/Cu(111) systems. The location of the Fermi level is indicated by a dashed vertical line at 0 eV. Arrows directed up and down indicate the up-spin and down-spin DOS, respectively. A Gaussian broadening of half-width 0.1 eV has been used.

of the gap states of h-BN adsorbed on Ni(111), Rh(111) and Pt(111) surfaces has been recently proved experimentally and explained by the orbital mixing and electron sharing at the interface [35]. In the case of Cu(111) surface the PDOS of the supported h-BN monolayer is also modified, however not so strong as for the Ni(111) surface. One can note appearence of the gap states at the top of the valence band of h-BN supported on Cu(111), as it is seen in Figure 2. We have also found a slight protrusion of the unoccupied BN states towards the Fermi level, clearly seen in the case of Cu(111) support. Therefore one can conclude that the changes in PDOS of h-BN deposited on transition metal surfaces correlate with the strength of the h-BN-metal bonding, as it was already mentioned in [37].

The features of the electronic structure of h-BN monolayer supported on transition metal surfaces can affect the process of O_2 adsorption and activation. Indeed, the catalytic activation of the adsorbed O_2 is related to an electron transfer from the support to the anti-bonding $2\pi^*$ orbital of oxygen. Presence of defect levels or the gap states nearby the Fermi level can promote the electron transfer from the support to the adsorbed O_2 and hence result in its catalytic activation.

3.2 Adsorption of O_2 on a free and metal supported h-BN monolayer.

In order to understand how the metal support can affect the chemical properties of the h-BN monolayer we consider adsorption of the molecular oxygen on the stand-alone pristine h-BN monolayer, h-BN/Ni(111) and h-BN/Cu(111) systems.

Our calculations demonstrate that molecular oxygen physisorbs on the defect-free h-BN monolayer in a configuration where the O−O bond is oriented parallel to the surface plane at the distance of 3 Å above the surface, as it is shown in Figure 3. The physisorbed oxygen remains catalytically non-activated in its triplet state with the binding energy of 0.06 eV to the h-BN monolayer. Here, the binding energy of O_2 to h-BN is defined as

$$E_b = E_{tot}(O_2) + E_{tot}(\text{h−BN}) - E_{tot}(O_2/\text{h−BN}), \quad (1)$$

where $E_{tot}(O_2/\text{h-BN})$ denotes the total energy of the O_2/h-BN system, while $E_{tot}(O_2)$ and $E_{tot}(\text{h-BN})$ are the energies of the non-interacting fully optimized O_2 and h-BN subsystems, respectively.

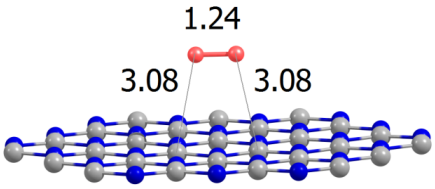

Fig. 3 Optimized structure of the molecular oxygen physisorbed on a free h-BN monolayer. The distances are given in Angstroms.

The weak interaction of O_2 with the pristine h-BN monolayer is expected, as the defect-free h-BN is chemically inert material. However, Ni(111) support

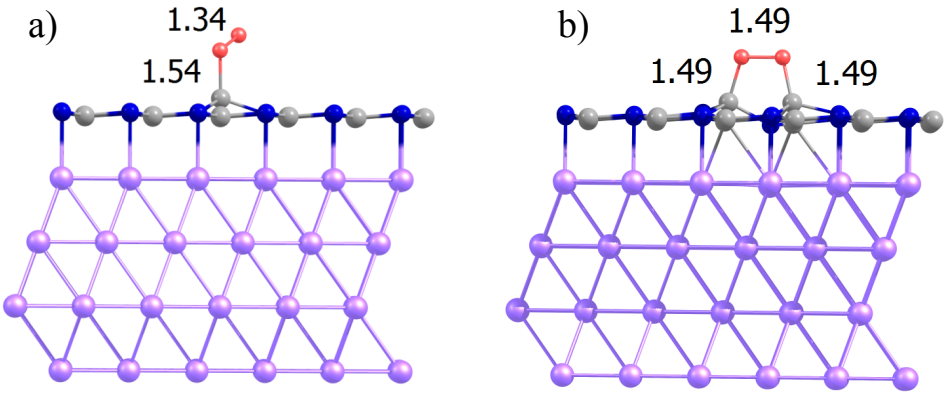

Fig. 4 Optimized structure of the molecular oxygen chemisorbed on the h-BN/Ni(111) surface in (a) on-top (in a doublet spin state) and (b) bridge configuration (in a singlet spin state). The distances are given in Angstroms.

strongly affects the chemical properties of h-BN monolayer and its ability to adsorb simple molecules. The results of our calculations show that molecular O_2 readily adsorbs on h-BN/Ni(111) in a top configuration (in a doublet spin state) with E_b = 0.64 eV and in a bridge configuration (in a singlet spin state) with E_b = 1.51 eV, as shown in Figures 4a and 4b, respectively. We also found the dissociative state of oxygen on the h-BN/Ni(111) surface with the binding energy of E_b = 0.60 eV, which is smaller than E_b calculated for the molecular adsorption of O_2. Therefore, one can suggest that O_2 dissociation is not favorable energetically on h-BN/Ni(111) surface. Similar conclusion has been made for the N-doped h-BN system [13].

In the top-configuration (Figure 4a), O_2 adsorbs on top of the B atom on the h-BN/Ni(111) surface and inclined from the surface normal, while in the bridge-configuration (Figure 4b) O_2 is oriented parallel to the surface and bridges two B atoms. In both cases the h-BN monolayer possesses structural relaxations upon O_2 adsorption. Thus, the B atoms localized in the vicinity of the adsorbed O_2 protrude above the surface plane by $\sim$ 0.5 Å. Strong interaction of O_2 with h-BN/Ni(111) results in the catalytic activation of the adsorbed O_2 and weakening of the O−O bond. The O−O bond length in O_2 adsorbed on h-BN/Ni(111) in on top configuration (Figure 4a) is elongated to 1.34 Å, similar to the superoxide state of oxygen (the O−O bond distances in O_2^- is 1.33 Å[20]), while in the case of a bridge configuration the O−O bond length elongated to 1.49 Å, similar to the peroxide state of oxygen (O_2^{2-}).

It is interesting that adsorption preferences of O_2 on h-BN/Cu(111) and h-BN/Ni(111) surfaces are is very similar. Figures 5a) and 5b) demonstrate that O_2 adsorbs in the top-configuration on top of the B atom on the h-BN/Cu(111) surface with E_b= 0.61 eV and in the B-B bridge-configuration parallel to the surface, with the binding energy of 1.54 eV. Interaction of O_2 with h-BN/Cu(111) results in the catalytic activation of the adsorbed O_2 and weakening of the O−O bond, similar to the case of h-BN/Ni(111) surface. However, structural deformations in h-BN monolayer upon O_2 adsorption are rather different for Ni(111) and Cu(111)

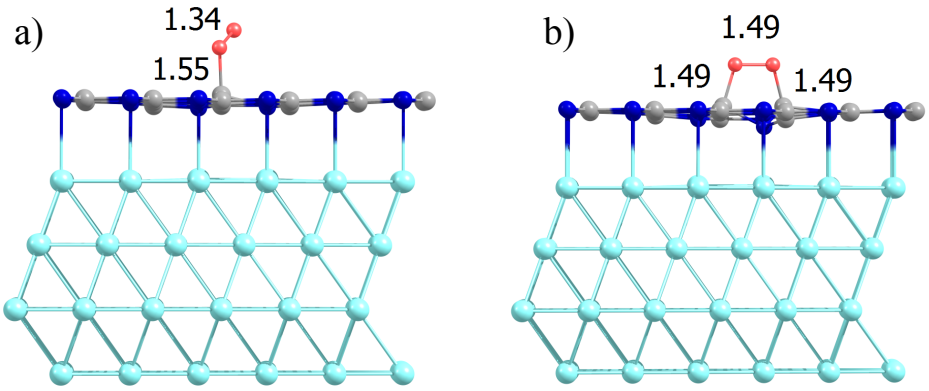

Fig. 5 Optimized structure of the molecular oxygen chemisorbed on the h-BN/Cu(111) surface in (a) on-top (in a doublet spin state) and (b) bridge configuration (in a singlet spin state). The distances are given in Angstroms.

supports. As it was discussed above, in the case of h-BN/Ni(111) system B atoms participating in the bonding with O_2 protrude above the h-BN surface plane by $\sim$ 0.5 Å. However, in the case of h-BN/Cu(111) system, these B atoms protrude above the surface only by $\sim$ 0.15 Å, while N atoms nearest to the adsorbed O_2 dip below the h-BN surface by $\sim$ 0.3 - 0.6 Å. Such deformation results in decrease of the Cu–N bond length for N atoms in the vicinity of the adsorbed O_2 and in increase of the strength of h-BN - Cu interaction. Thus, adsorption of O_2 on h-BN/Cu(111) promotes binding of h-BN to the Cu(111) surface. The flexibility of the h-BN monolayer is crucial for the strong adsorption of O_2 on h-BN/Cu(111).

In order to clarify mechanism of O_2 activation on the metal supported h-BN monolayer we present analysis of the partial density of electronic states of the adsorbed oxygen. The maxima of the PDOS corresponding to the O_2 molecule adsorbed on the h-BN and h-BN/metal surfaces can be assigned to the peaks of the PDOS spectra of the free O_2. Oxygen molecule possesses the occupied up-spin antibonding $2\pi^*$ orbital below the Fermi level and the unoccupied down-spin $2\pi^*$ orbital above the Fermi level.

Figure 6a demonstrates that in the case of O_2 physisorption on the pristine h-BN monolayer the spin-polarized PDOS spectrum of O_2 remains unperturbed by the weak interaction with the support. However, when O_2 adsorbs on the h-BN/Ni(111) surface one can see a considerable change in PDOS spectra. As it was discussed above, the interaction of h-BN monolayer with the Ni(111) substrate results in formation of the gap states in h-BN with p_z character. These gap states are located in the same energy region as the antibonding O_2-$2\pi^*$ orbitals, and strongly mixed with each other. Figure 6b demonstrates that in the case of on top adsorption of the molecular oxygen on h-BN/Ni(111) the O_2-$2\pi^*$ orbitals split into two components, which lie in the plane and perpendicular to the plane defined by the O_2 and B atom. The down-spin $2\pi^*$ orbital of a free or physisorbed O_2 is unoccupied and located above the Fermi level. Adsorption of O_2 on top of B atom on h-BN/Ni(111) leads to the appearance of the partly filled down-spin $2\pi^*$ component in the PDOS spectra, below the Fermi level, as shown in Figure 6b.

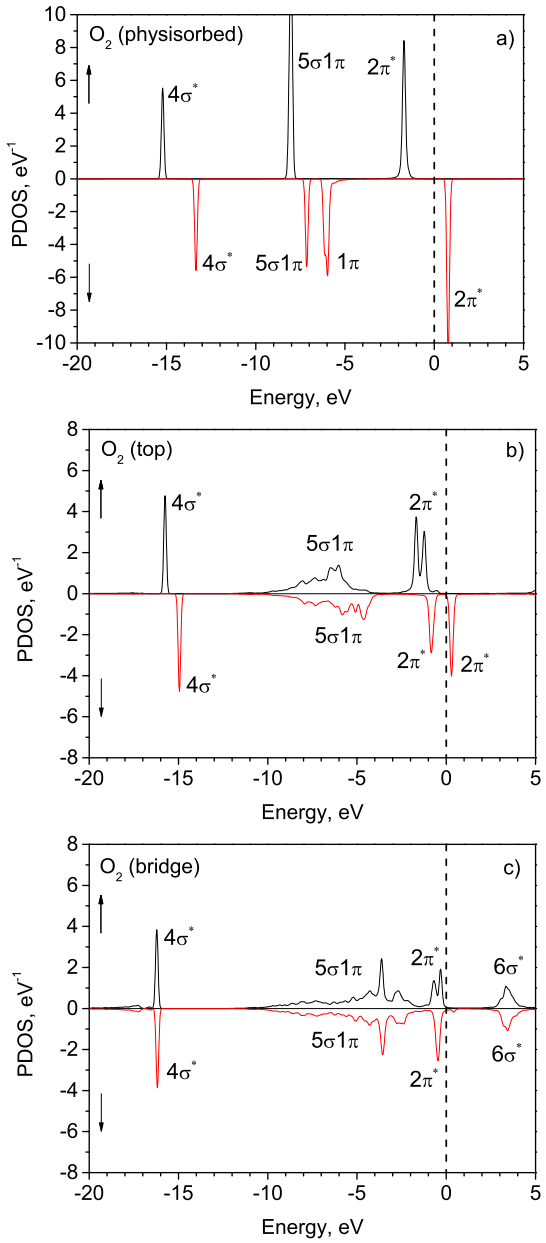

Fig. 6 Partial density of electronic states (PDOS) projected on the O_2 molecule (a) physisorbed on h-BN monolayer, and adsorbed on the h-BN/Ni(111) surface in the (b) top (superoxo-like) and (c) bridge (peroxo-like) configurations. The position of the Fermi level is indicated by a dashed vertical line at 0 eV. Arrows directed up and down indicate the up-spin and down-spin PDOS, respectively. Gaussian broadening of half-width 0.1 eV has been used.

One can also notice a prominent broadening of O_2-$5\sigma 1\pi$ orbitals due to the strong interaction with the support. Partial population of the antibonding $2\pi^*$ orbital of O_2 is responsible for the catalytic activation of the adsorbed oxygen and stretching of the O–O bond. According to the Bader analysis, the charge localized on the O_2 adsorbed in on-top configuration is -0.92e, where e is an elementary charge. Such mechanism of the charge-transfer-mediated activation of O_2 has been intensively studied for O_2 adsorbed on metal clusters; see, *e.g.*, refs [11, 16, 17, 19, 21–27] and references therein. Adsorption of O_2 on h-BN/Ni(111) in a bridge configuration results in a further population of the down-spin $2\pi^*$ orbital which becomes completely occupied and lies below the Fermi level. There is no considerable spin polarization of O_2 orbitals. The calculated Bader charge localized on O_2 adsorbed in the bridge configuration is -1.81 e, which confirms that this configuration corresponds to the highly reactive peroxide state. The mechanism of O_2 activation on the h-BN/Cu(111) support is very similar to that described for h-BN/Ni(111).

It is interesting to compare adsorption of O_2 to h-BN/Ni(111) and h-BN/Cu(111) supports with the case of the pure Ni(111) and Cu(111) surfaces. Earlier theoretical calculations have determined two molecular configurations of O_2 on Ni(111) surface when O_2 adsorbs at the bridge-site with two atoms oriented towards the neighboring substrate atoms (top-bridge-top configuration), and at the threefold hollows (fcc or hcp), when the molecule stretching from top to bridge (top-hollow-bridge configuration) [75]. The binding energies of O_2 to Ni(111) are 1.34-1.41 and 1.55-1.67 eV, calculated for the top-bridge-top and top-hollow-bridge configuration, respectively [75, 76]. In the case of Cu(111) surface O_2 binds to the surface in a paramagnetic superoxo-like state, O_2^-, adsorbed in a flat top-bridge-top geometry with the binding energy of 0.45 eV, and in a nonmagnetic peroxo-like state, O_2^{2-}, adsorbed in a bridge-hollow-bridge configuration with the binding energy 0.56 eV [77]. The results of our calculations demonstrate that in the case of O_2 adsorption on h-BN/Ni(111) and h-BN/Cu(111) systems there are two possible configurations of O_2, corresponding to the superoxo-like and peroxo-like states, similar to adsorption on Ni(111) and Cu(111). The superoxo-like state of O_2 on h-BN/Ni(111) has considerably smaller binding energy if compared with the pure Ni(111) surface. On the other hand the peroxo-like state of O_2 on h-BN/Ni(111) has the binding energy similar to that calculated for Ni(111). In the case of h-BN/Cu(111) support the superoxo-like state of O_2 on h-BN/Cu(111) has the binding energy to the surface similar to the superoxo-like state of O_2 on Cu(111), however the peroxo-like state of O_2 binds to h-BN/Cu(111) considerably stronger than to the pure Cu(111) surface.

4 Conclusions

In conclusion, we have reported results of the theoretical calculations of O_2 adsorption and activation on the stand-alone and the metal supported h-BN monolayer. It is demonstrated that inert h-BN monolayer can be functionalized by the metal support and become active for O_2 activation. It is shown that O_2 adsorbs on h-BN/Ni(111) and h-BN/Cu(111) systems in two configurations, corresponding to the superoxo-like and peroxo-like states of oxygen. It is shown that the metal substrate influences the molecular adsorption and chemical reactions on the supported h-BN surface via the mixing between metal d and h-BN π bands. Such an

effect can open a new way to tune adsorption characteristics of O_2 and reactant molecules on h-BN by the selection of metal substrate.

References

1. M. Haruta, Nature 437 (2005) 1098–1099.
2. S. E. Davis, M. S. Ide, R. J. Davis, Green Chem. 15 (2013) 17–45.
3. U. Heiz, U. Landman (Eds.), Nanocatalysis, Springer, Berlin, Heidelberg, New York, 2007.
4. M. Haruta, T. Kobayashi, H. Sano, N. Yamada, Chem. Lett. 16 (1987) 405–408.
5. M. Haruta, Catal. Today 36 (1997) 153–166.
6. M. Turner, V. B. Golovko, O. P. H. Vaughan, P. Abdulkin, A. Berenguer-Murcia, M. S. Tikhov, B. F. G. Johnson, R. M. Lambert, Nature 454 (2008) 981–984.
7. M. D. Hughes, Y.-J. Xu, P. Jenkins, P. McMorn, P. Landon, D. I. Enache, A. F. Carley, G. A. Attard, G. J. Hutchings, F. King, E. H. Stitt, P. Johnston, K. Griffin, C. J. Kiely, Nature 437 (2005) 1132–1135.
8. H. Tsunoyama, H. Sakurai, Y. Negishi, T. Tsukuda, J. Am. Chem. Soc. 127 (2005) 9374–9375.
9. P. Landon, P. J. Collier, A. J. Papworth, C. J. Kiely, G. Hutchings, Chem. Commun. (2002) 2058–2059.
10. A. A. Herzing, C. J. Kiely, A. F. Carley, P. Landon, G. J. Hutchings, Science 321 (2008) 1331–1335.
11. A. Lyalin, T. Taketsugu, J. Phys. Chem. C 113 (2009) 12930–12934.
12. A. Lyalin, T. Taketsugu, J. Phys. Chem. Lett. 1 (2010) 1752–1757.
13. A. Lyalin, A. Nakayama, K. Uosaki, T. Taketsugu, Phys. Chem. Chem. Phys. 15 (2013) 2809–2820.
14. H. Zeng, C. Zhi, Z. Zhang, X. Wei, X. Wang, W. Guo, Y. Bando, D. Golberg, Nano Lett. 10 (2010) 5049–5055.
15. S. Azevedo, J. R. Kaschny, C. M. de Castilho, F. de Brito Mota, Eur. Phys. J. B 67 (2009) 507–512.
16. M. Gao, A. Lyalin, T. Taketsugu, J. Phys. Chem. C 116 (2012) 9054–9062.
17. M. Gao, A. Lyalin, T. Taketsugu, Int. J. Quantum Chem. 113 (2013) 443–452.
18. M. Gao, A. Lyalin, T. Taketsugu, Catalysts 1 (2011) 18–39.
19. M. Gao, A. Lyalin, T. Taketsugu, J. Chem. Phys. 138 (2013) 034701.
20. N. Wiberg, A. F. Holleman, E. Wiberg (Eds.), Inorganic Chemistry, Academic Press, 2001.
21. H. Häkkinen, U. Landman, J. Am. Chem. Soc. 123 (2001) 9704–9705.
22. L. D. Socaciu, J. Hagen, T. M. Bernhardt, L. Wöste, U. Heiz, H. Häkkinen, U. Landman, J. Am. Chem. Soc. 125 (2003) 10437–10445.
23. H. Häkkinen, S. Abbet, A. Sanchez, U. Heiz, U. Landman, Angew. Chem. Int. Ed. 42 (2003) 1297–1300.
24. B. Yoon, H. Häkkinen, U. Landman, J. Phys. Chem. A 107 (2003) 4066–4071.
25. R. Coquet, K. L. Howard, D. J. Willock, Chem. Soc. Rev. 37 (2008) 2046–2076.
26. X. Ding, Z. Li, J. Yang, J. G. Hou, Q. Zhu, J. Chem. Phys. 120 (2004) 9594–9600.
27. E. Fernández, P. Ordejón, L. C. Balbás, Chem. Phys. Lett. 408 (2005) 252–257.

28. J. Gómez Díaz, Y. Ding, R. Koitz, A. P. Seitsonen, M. Iannuzzi, J. Hutter, Theor. Chem. Acc. 132 (2013) 1350.
29. Y. Lin, J. W. Connell, Nanoscale 4 (2012) 6908–6939.
30. L. Britnell, R. V. Gorbachev, R. Jalil, B. D. Belle, F. Schedin, M. I. Katsnelson, L. Eaves, S. V. Morozov, A. S. Mayorov, N. M. R. Peres, A. H. Castro Neto, J. Leist, A. K. Geim, L. A. Ponomarenko, K. S. Novoselov, Nano Lett. 12 (2012) 1707–1710.
31. A. Nagashima, N. Tejima, Y. Gamou, T. Kawai, C. Oshima, Phys. Rev. B 51 (1995) 4606–4613.
32. E. Rokuta, Y. Hasegawa, K. Suzuki, Y. Gamou, C. Oshima, A. Nagashima, Phys. Rev. Lett. 79 (1997) 4609–4612.
33. A. B. Preobrajenski, A. S. Vinogradov, N. Mårtensson, Phys. Rev. B 70 (2004) 165404.
34. A. B. Preobrajenski, A. S. Vinogradov, N. Mårtensson, Surf. Sci. 582 (2005) 21–30.
35. A. B. Preobrajenski, S. A. Krasnikov, A. S. Vinogradov, M. L. Ng, T. Käämbre, A. A. Cafolla, N. Mårtensson, Phys. Rev. B 77 (2008) 085421.
36. R. Laskowski, T. Gallauner, P. Blaha, K. Schwarz, J. Phys.: Condens. Matter 21 (2009) 104210.
37. R. Laskowski, P. Blaha, K. Schwarz, Phys. Rev. B 78 (2008) 045409/1–10.
38. G. B. Grad, P. Blaha, K. Schwarz, W. Auwärter, T. Greber, Phys. Rev. B 68 (2003) 085404.
39. M. N. Huda, L. Kleinman, Phys. Rev. B 74 (2006) 075418.
40. T. Brugger, S. Günther, B. Wang, J. H. Dil, M.-L. Bocquet, J. Osterwalder, J. Wintterlin, T. Greber, Phys. Rev. B 79 (2009) 045407.
41. I. Shimoyama, Y. Baba, T. Sekiguchi, K. Nath, J. Electron Spectrosc. Relat. Phenom. 175 (2009) 6–13.
42. Y. Zhou, X. Zu, F. Gao, Solid State Commun. 151 (2011) 883–886.
43. Z. Wu, R. E. Cohen, Phys. Rev. B 73 (2006) 235116/1–6.
44. F. Tran, R. Laskowski, P. Blaha, K. Schwarz, Phys. Rev. B 75 (2007) 115131.
45. R. Laskowski, P. Blaha, Phys. Rev. B 81 (2010) 075418.
46. E. Artacho, D. Sánchez-Portal, P. Ordejón, A. García, J. M. Soler, Phys. Stat. Sol. (b) 215 (1999) 809–817.
47. J. Junquera, O. Paz, D. Sánchez-Portal, E. Artacho, Phys. Rev. B 64 (2001) 235111/1–9.
48. N. Troullier, J. L. Martins, Phys. Rev. B 43 (1991) 1993–2006.
49. L. Kleinman, D. M. Bylander, Phys. Rev. Lett. 48 (1982) 1425–1428.
50. D. Sánchez-Portal, P. Ordejón, E. Artacho, J. M. Soler, Int. J. Quantum Chem. 65 (1997) 453–461.
51. J. M. Soler, E. Artacho, J. D. Gale, A. García, J. Junquera, P. Ordejón, D. Sánchez-Portal, J. Phys.: Condens. Matter 14 (2002) 2745–2779.
52. D. Sánchez-Portal, P. Ordejón, E. Canadell, Structure and Bonding 113 (2004) 103–170.
53. H. J. Monkhorst, J. D. Pack, Phys. Rev. B 13 (1976) 5188.
54. C. S. Yoo, J. Akella, H. Cynn, M. Nicol, Phys. Rev. B 56 (1997) 140–146.
55. R. W. G. Wyckoff, Crystal Structures, Vol. 1, John Wiley & Sons, 1963.
56. M. E. Straumanis, L. S. Yu, Acta Crystallogr. 25A (1969) 676–682.
57. R. Bader, Atoms in Molecules: A Quantum Theory, Oxford University Press, New York, 1990.

58. G. Henkelman, A. Arnaldsson, H. Jónsson, Comput. Mater. Sci. 36 (2006) 354–360.
59. A. Lyalin, T. Taketsugu, J. Phys. Chem. C 114 (2010) 2484–2493.
60. A. Lyalin, T. Taketsugu, Faraday Discuss. 152 (2011) 185–201.
61. A. Lyalin, I. A. Solov'yov, A. V. Solov'yov, W. Greiner, Phys. Rev. A 67 (2003) 063203.
62. A. Lyalin, I. A. Solov'yov, A. V. Solov'yov, W. Greiner, Phys. Rev. A 75 (2007) 053201.
63. A. Lyalin, A. V. Solov'yov, W. Greiner, Phys. Rev. A 74 (2006) 043201.
64. J. P. Connerade, A. G. Lyalin, R. Semaoune, S. K. Semenov, A. V. Solov'yov, J. Phys. B: At., Mol. Opt. Phys. 34 (2001) 2505–2511.
65. V. V. Semenikhina, A. Lyalin, A. V. Solov'yov, W. Greiner, JETP 106 (2008) 678–689.
66. J. G. Che, H.-P. Cheng, Phys. Rev. B 72 (2005) 115436.
67. J. Rusz, A. B. Preobrajenski, M. L. Ng, N. A. Vinogradov, N. Mårtensson, O. Wessely, B. Sanyal, O. Eriksson, Phys. Rev. B 81 (2010) 073402.
68. C. Oshima, A. Itoh, E. Rokuta, T. Tanaka, K. Yamashita, T. Sakurai, Solid State Commun 116 (2000) 37–40.
69. Y. Zhang, W. Yang, Phys. Rev. Lett. 80 (1998) 890–890.
70. S. Grimme, J. Antony, S. Ehrlich, H. Krieg, J. Chem. Phys. 132 (2010) 154104.
71. S. Joshi, D. Ecija, R. Koitz, M. Iannuzzi, A. P. Seitsonen, J. Hutter, H. Sachdev, S. Vijayaraghavan, F. Bischoff, K. Seufert, J. V. Barth, W. Auwärter, Nano Lett. 12 (2012) 5821–5828.
72. C. Oshima, A. Nagashima, J. Phys.: Condens. Matter 9 (1997) 1–20.
73. M. Muntwiler, W. Auwärter, F. Baumberger, M. Hoesch, T. Greber, J. Osterwalder, Surf. Sci. 472 (2001) 125–132.
74. V. Solozhenko, A. Lazarenko, J.-P. Petitet, A. Kanaev, J. Phys. Chem. Solids 62 (2001) 1331 – 1334.
75. F. Mittendorfer, A. Eichler, J. Hafner, Surf. Sci. 433-435 (1999) 756–760.
76. C.-H. Yeh, J.-J. Ho, ChemPhysChem 13 (2012) 3194–3203.
77. Y. Xu, M. Mavrikakis, Surf. Sci. 494 (2001) 131–144.